



Assessment of a novel photovoltaic electrolyzer fuel cell-ORC hybrid energy system for hydrogen and power production

M. Rahimi-Esbo^{1,*} | M. Rezaei Firouzjaee² | H. Bagherian Farahabadi¹ | E. Alizadeh³

¹Assistant professor, Northern Research Center for Science & Technology, Malek Ashtar University of Technology, Iran

²Researcher, Northern Research Center for Science & Technology, Malek Ashtar University of Technology, Iran

³Associated professor, Northern Research Center for Science & Technology, Malek Ashtar University of Technology, Iran

*Corresponding author, mrahimi@mut.ac.ir

Article Information

Article Type:

Research Article

Article History:

Received: 15 March 2023

Received in revised form
15 May 2023

Accepted: 12 June 2023

Published on line 20 June
2023

Keywords

Solar energy

Organic Rankine cycle (ORC)

PEM fuel cell (PEMFC)

PEM electrolyzer (PEME)

Photovoltaics (PV) cell

Hydrogen production

Abstract

This study aimed to explore new insights within the realm of hybrid renewable energy systems specifically designed for off-grid applications, using a combination of numerical simulations and real-world experiments. The system described in the study was developed to cater to the electricity needs of a telecommunications tower. It was achieved by integrating various components, including a photovoltaic (PV) unit, a proton exchange membrane electrolyzer (PEME), a proton exchange membrane fuel cell (PEMFC), and a battery storage unit. Additionally, an Organic Rankine Cycle (ORC) system was integrated to efficiently capture and utilize waste heat generated by the PEMFC. In this setup, the PV unit serves as the primary power source, with any excess solar energy being directed toward the PEME during periods of high solar irradiation. The PEME then converts this surplus energy into hydrogen and oxygen. Subsequently, the PEMFC utilizes the hydrogen stored in metal hydride tanks to generate electricity, thus ensuring a continuous and reliable power supply for the telecom tower. Results indicate that an optimal ORC turbine inlet pressure of approximately 600 kPa maximizes overall exergy and energy efficiencies by 53.2% and 50.9%, respectively.

Cite this article: Rahimi-Esbo, M., Rezaei Firouzjaee, M., Bagherian Farahabadi, H., Alizadeh, E. (2023). Assessment of a novel photovoltaic electrolyzer fuel cell-ORC hybrid energy system for hydrogen and power production. DOI:10.22104/HFE.2023.6527.1269



© The Author(s).

Publisher: Iranian Research Organization for Science and Technology (IROST)

DOI: 10.22104/HFE.2023.6527.1269

1. Introduction

The global challenge of combating climate change is of the utmost importance to nations worldwide. The primary cause of the emission of greenhouse gases is the extensive use of fossil fuels for transportation, power generation, and heating. A fundamental reevaluation of our energy systems is imperative to achieve net-zero carbon emissions. In this pursuit, integrating renewable energy sources like wind and solar power plays a pivotal role [1]. Abundant and environmentally friendly solar energy can be harnessed for electricity generation, heating, and lighting. Its benefits include reducing greenhouse gas emissions, energy self-sufficiency, and economic advantages [2]. However, solar power generation is weather-dependent, necessitating energy storage solutions. Hydrogen, as an eco-friendly energy carrier, presents a promising avenue for storing surplus electricity from renewables. Due to hydrogen's clean fuel properties, straightforward operations, low-temperature requirements, and high-purity end products, solar hydrogen production holds substantial promise [3, 4].

Multiple techniques exist for hydrogen production, with a shift towards renewable energy sources instead of fossil fuels. Solar-driven water electrolysis for hydrogen production has emerged as a compelling framework for sustainable energy. Photovoltaic (PV) systems are particularly attractive due to their direct conversion of sunlight into electricity, environmental benefits, modularity, low maintenance, and long lifespan. Exploring cooling strategies for PV thermal systems can enhance their performance [5]. Hybrid renewable energy systems are gaining prominence, bolstering power quality through combined energy storage solutions. During periods of low electricity demand, excess power from PV systems can be used to produce hydrogen through water electrolysis. The integration of hybrid PV, fuel cells, and electrolyzers enhances the reliability of renewable energy setups

[6, 7].

Fuel cells, which efficiently convert hydrogen into power, offer several advantages, such as quick adaptation to changing loads, fast activation, low operating temperatures, high power density, and reduced emissions. Proton exchange membrane fuel cells (PEMFCs) are favored for their versatility, particularly when integrated with high-purity hydrogen production through proton exchange membrane electrolyzers (PEMEs) [8, 9]. Recent research has focused on analyzing hybrid renewable energy systems. Studies have assessed the techno-economic viability of systems incorporating PV, battery storage, fuel cells, electrolyzers, and biogas. Sizing investigations are crucial in determining the optimal component sizes for system self-reliance and sustained functionality. Capacity loss in components has also been explored, revealing strategies to extend battery life and optimize system efficiency [10-12].

This research marks a pioneering effort as it is the first study to employ an Organic Rankine Cycle (ORC) for the purpose of recovering waste heat within a hybrid renewable energy system. Its novelty lies in its all-encompassing approach, advanced research methods, incorporation of various renewable components (notably the fuel cell), and rigorous experimental validation, signifying a noteworthy progression in the domain of hybrid energy systems.

2. Experimental

Figure 1 provides a visual representation of the proposed hybrid energy system, illustrating the arrangement of its various components. This comprehensive system includes photovoltaic (PV) panels, a proton exchange membrane electrolyzer (PEME), a proton exchange membrane fuel cell (PEMFC) stack, an organic Rankine cycle (ORC), a battery bank, hydrogen and oxygen storage tanks, a hydrogen compressor, an inverter, and the telecommunication tower. The prima-

ry power source in this system is the PV unit, which utilizes maximum power point tracking (MPPT) solar charge controllers to optimize its performance. When solar irradiation exceeds the telecom tower’s electricity demand, surplus power is directed to the PEM electrolyzer, producing hydrogen and oxygen for storage. PEM electrolyzers are preferred for their safety, compactness, and high current density. The PEM fuel cell is fueled by hydrogen (from metal hydride tanks) and oxygen (from a storage tank), providing consistent electrical power regardless of environmental condi-

tions. Excess heat generated by the PEMFC is effectively utilized by the ORC as a low-grade heat source. Batteries play a crucial role in storing energy generated by PV and PEMFC for short-term use. When solar irradiation is insufficient to meet demand, batteries compensate for the shortfall. To optimize battery performance and lifespan, the PEMFC is activated when the battery’s state of charge falls below a threshold and deactivated when the storage system reaches full charge.

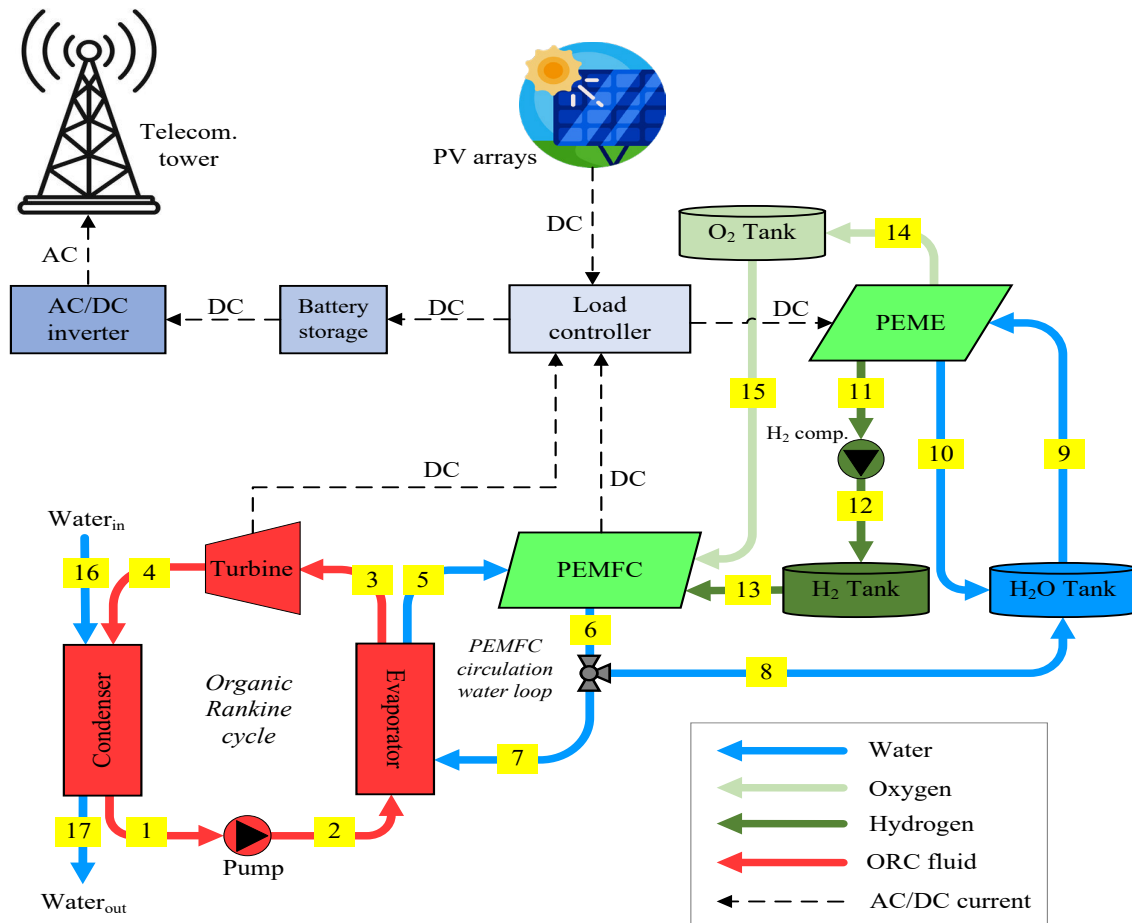
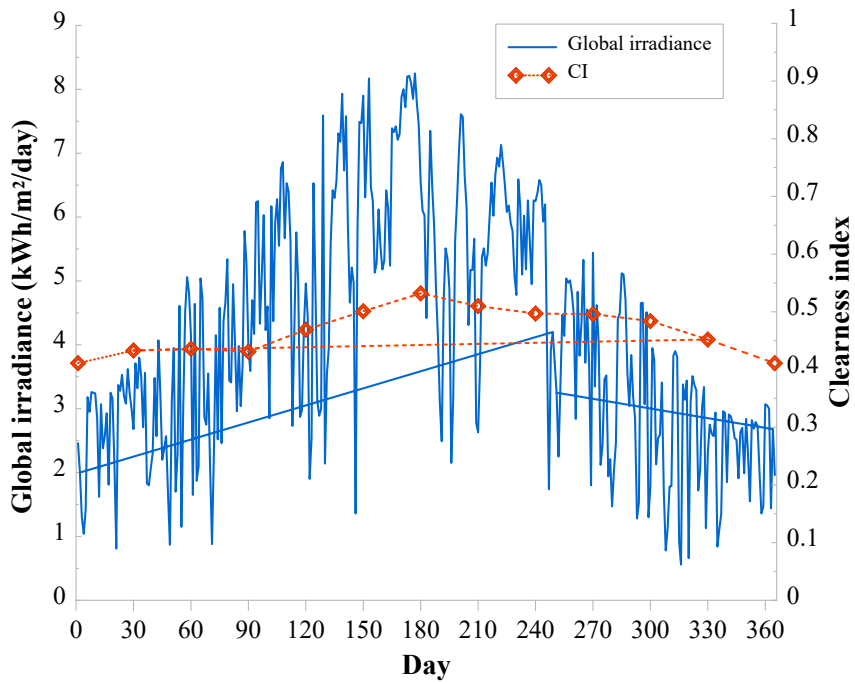


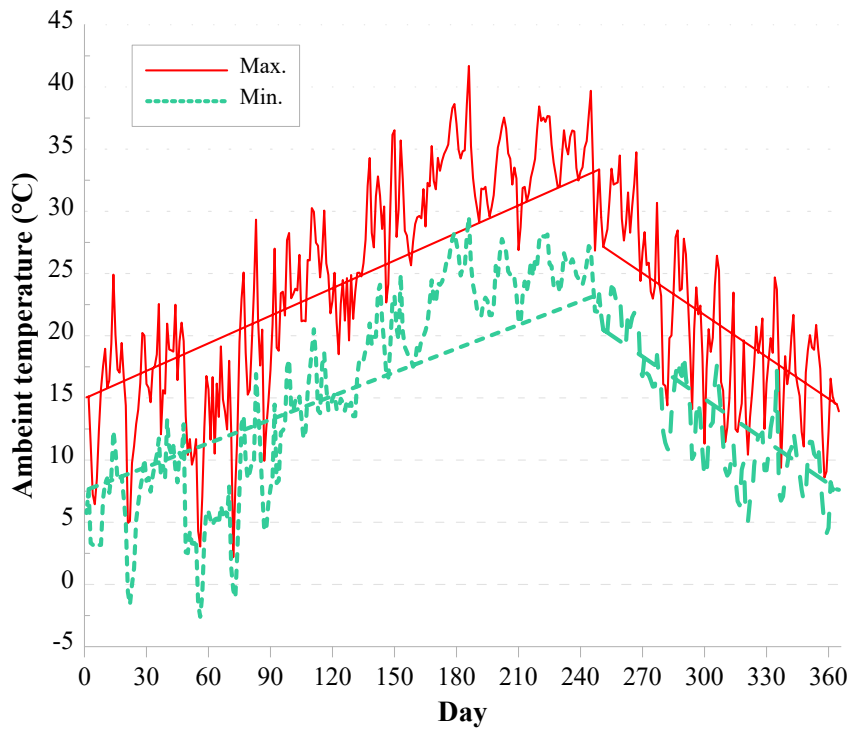
Fig.1. Configuration of the proposed hybrid energy system.

The simulation model uses real weather data from (2022) in Babolsar, Iran (located at 36°42'3"N, 52°38'53"E). Fig. 2(a) displays global solar irradiation and clearness index, and Fig. 2(b) shows annual maximum and minimum ambient temperatures [13].

tion and clearness index, and Fig. 2(b) shows annual maximum and minimum ambient temperatures [13].



(a)



(b)

Fig. 2. (a) Global solar irradiance and clearness index (b) maximum and minimum temperature over the course of a year.

Fig. 3 illustrates the daily load demand for the telecom tower, with a target of around 50 kWh per

day and a peak power requirement of roughly 2.5 kW, serving as the basis for designing this hybrid energy system.

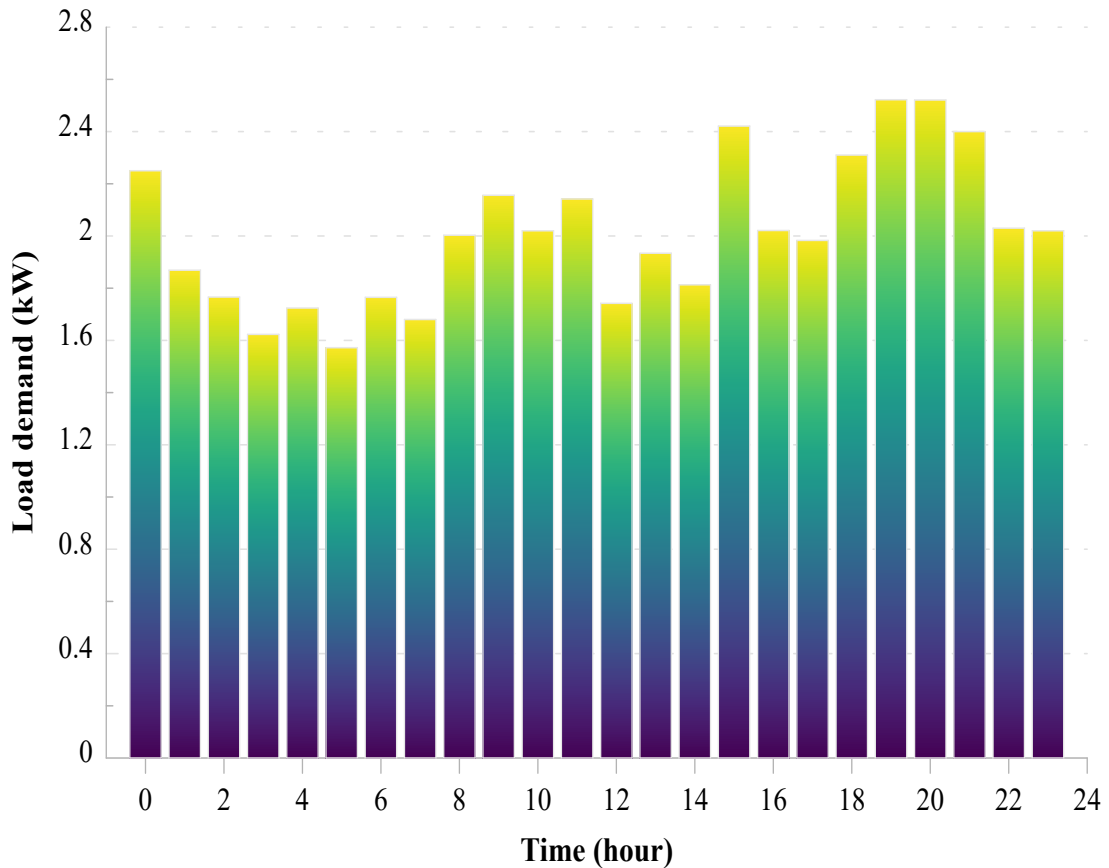
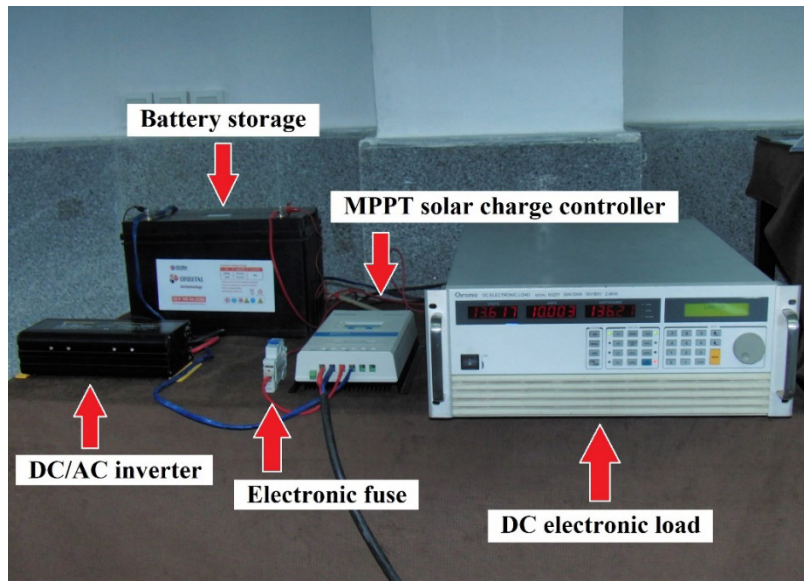


Fig. 3. Daily load demand of the telecom tower.

2.1. PV experimental setup & modeling

To prepare for numerical modeling of PV cells and gather empirical data, a series of experimental tests were conducted using Q.Cells' Q.Power G5 270W polycrystalline solar modules. Figure 4

provides a visual representation of the experimental setup, including two PV modules, a battery, an MPPT solar charge controller, an electronic load, an inverter, a fuse, and wiring. These tests were performed with the modules temporarily mounted at a fixed tilt angle of 33 degrees facing south.



(a)



(b)

Fig.4. (a) PV experimental setup and (b) PV modules.

The experiments involved measuring current-voltage relationships and calculating power-voltage characteristics under varying conditions throughout the day. Measured data and modeling accuracy assessments are presented in the following section for comparison with numerical results. The experiments also employed a DC electronic load to subject the PV modules

to specific loading conditions. Various instruments and equipment were used to measure parameters such as solar irradiation, module surface temperature, ambient temperature, current, voltage, etc., detailed in Tables 1 and 2. Additionally, a 100 Ah/12 V sealed lead-acid battery served as the energy storage unit for the hybrid energy system.

Table 1. Measuring Instruments for Experimental Tests

Model name	Purpose	Operating range	Accuracy
HIOKI clamp HiTESTer 3284	AC/DC current and voltage clamp meter	Current: 20 / 200 A Voltage: 30 to 600 V	Current: $\pm 1.3\%$ Voltage: $\pm 1.0\%$
HIOKI digital multimeter DT4282	AC/DC current and voltage multimeter	Current: 600 μ A to 10 A Voltage: 60 mV to 1000 V	Current: $\pm 0.05\%$ Voltage: $\pm 0.025\%$
TES 132 solar power meter	Solar radiation measurement	200 – 2000 W/m ²	± 1.0 W/m ²
Fluke 568 IR	Thermometer	-40 – 800 °C	± 1.0 °C

Table 2. Technical Specification of Q.Power-G5 270

Parameter	Value
Dimensions (mm)	1650 \times 991 \times 35
Area, A_{PV} (m ²)	1.63
Cells	6 \times 10
Weight (kg)	18 \pm 5%
Power at MPP, P_{MPP} (W)	270
Current at MPP, I_{MPP} (A)	8.69
Voltage at MPP, V_{mpp} (V)	31.1
Short circuit current, I_{sc} (A)	9.23
Open circuit voltage, V_{oc} (V)	38.1
Efficiency (%)	≥ 16.5
Temperature coefficient of I_{sc} (%/K)	0.05
Temperature coefficient of V_{oc} (%/K)	-0.31
Temperature coefficient of P_{MPP} (%/K)	-0.40

Fig. 5 displays observed ambient temperature and global solar irradiation data for a clear day in Babol-sar, Iran, on January 1st. At 2:00 PM, the highest val-

ues recorded were 953 W/m² for solar irradiation and 294.4 K for ambient temperature.

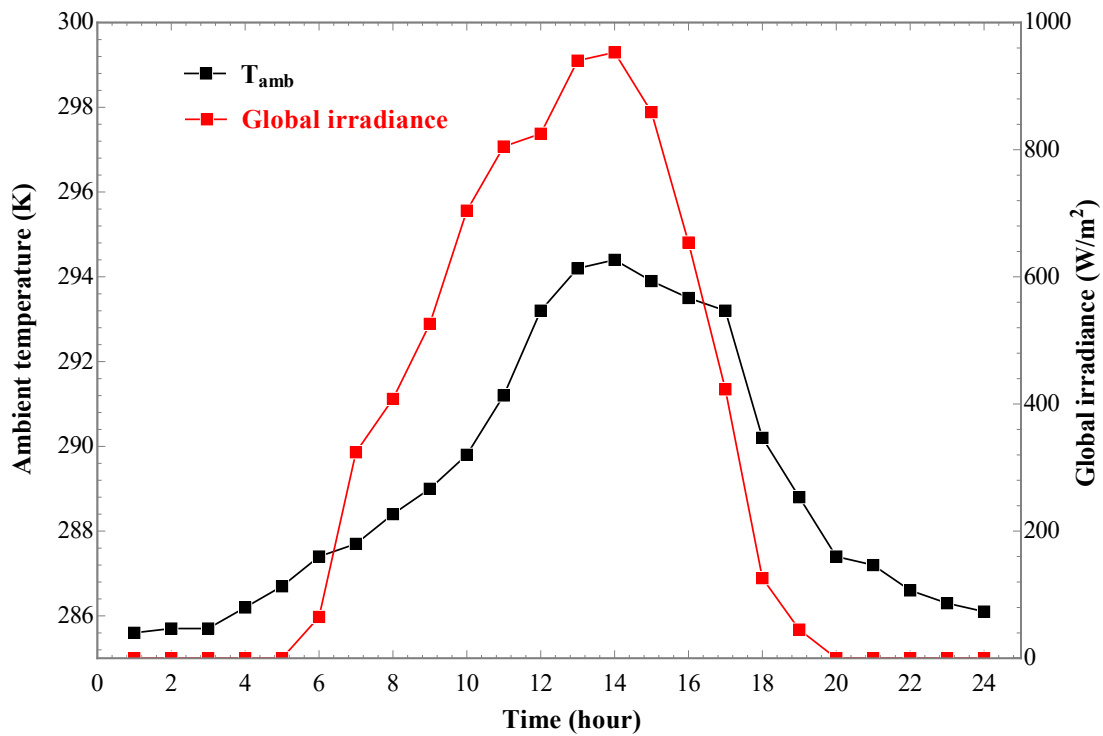


Fig. 5. Determined experimental data for global irradiance and ambient temperature.

In accordance with [14], the I-V curve of a PV cell at its maximum power point is commonly represented as follows:

(1)

$$I_{mp} = I_L - I_o \left[\exp\left(\frac{v_{mp} + I_{mp}R_s}{a}\right) - 1 \right] - \frac{v_{mp} + I_{mp}R_s}{R_{SH}}$$

Where, I_{mp} defines the maximum current, and V_{mp} shows the maximum voltage of the PV solar cell. I_o is defined as the diode reverse saturation current, I_L is the light-generated current (a specified ideality factor), and R_s and R_{SH} are series and shunt resistance, respectively. The maximum power of

the PV cell is calculated as follows:

$$P_{mp} = I_{mp}V_{mp} \tag{2}$$

Fig. 6 compares the experimental and numerical results of the PV cell power output, showing variations throughout the day due to ambient temperature and solar radiation. The peak power output aligns with maximum solar radiation around 2:00 PM. Notably, Fig. 6 illustrates the numerical model’s high precision, as it closely matches the experimental data.

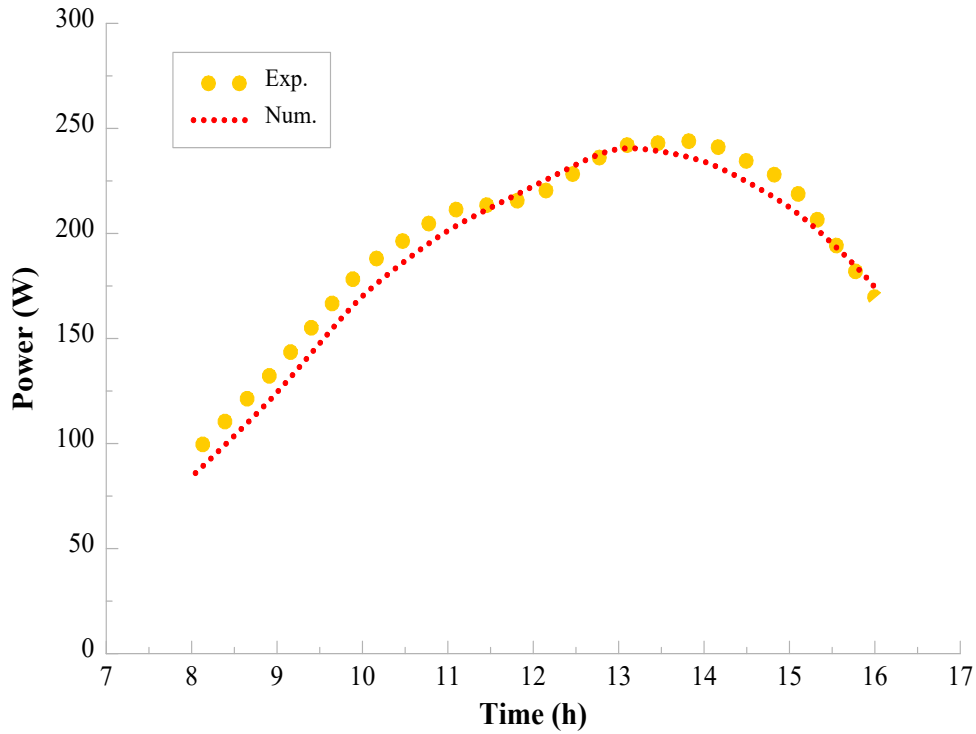


Fig. 6. Comparing numerical and experimental data results for PV cell output power.

2.2. Proton exchange membrane fuel cell (PEMFC) modeling

The produced power of a PEM fuel cell can be defined by [15]:

$$\dot{W}_{PEMFC} = V_{PEMFC} \cdot \dot{i}_{PEMFC} \tag{3}$$

Here, i_{PEMFC} denotes fuel cell current density, and the single-cell output voltage can be calculated as follows [16]:

$$V_{PEMFC} = N_c E_{cell} = N_c (E_{Nemst} - E_{Loss}) \tag{4}$$

Where, N_c and E_{Cell} define the number of cells and fuel cell voltage, respectively. The Nernst voltage, which is also known as the open circuit voltage of PEMFC, is described as the highest voltage generated by the

cell and can be determined by:

$$E_{Nemst} = 1.229 - 0.85e^{-3}(T - T_0) + 4.31e^{-5}T \left[\ln(P_{H_2} P_{O_2}^{0.5}) \right] \tag{5}$$

Here, T is the operating temperature of the fuel cell, T_0 is defined as the dead state temperature, and P_{H_2} and P_{O_2} represent the partial pressure of hydrogen and oxygen, respectively. The voltage losses can be estimated in a parametric relation by [17]:

$$E_{Loss} = E_{Act} + E_{Con} + E_{Ohm} \tag{6}$$

The activation loss is estimated by:

$$E_{Act} = T_{PEMFC} (m + n \cdot (i_{PEMFC})) \tag{7}$$

By using the following equation, the concentration loss is computed:

$$E_{Con} = 0.06 \ln \left(1 - \frac{i_{PEMFC}}{i_{Max}} \right) \quad (8)$$

The ohmic loss is formulated by:

$$E_{Ohm} = -i_{PEMFC} R_{Ohm} = i_{PEMFC} (R_{Ohm0} + R_{Ohm1}) \quad (9)$$

Here, i_{Max} is specified as the maximum available value of i_{PEMFC} , R_{Ohm0} and R_{Ohm1} represent equivalent inner and outer membrane resistance, respectively, and semi-empirical coefficients are introduced by m and n . The inputs and operating parameters of the PEM fuel cell are provided in Table 3.

Table 3. Input Parameters for the PEM Fuel Cell

Parameter	Value
Current density, i_{pemfc} (A/cm ²)	0.6
Cell numbers, N_c	60
Operating temperature, T_{PEMFC} (K)	360
Operating pressure, P_{PEMFC} (kPa)	101
Active surface area, A_{pemfc} (cm ²)	232
Membrane thickness (cm)	0.018
Limiting current density (A/cm ²)	2.0
Hydrogen stoichiometric ratio, λ_{H_2}	1.2
Oxygen stoichiometric ratio, λ_{O_2}	2
Faraday constant, F (C/mol)	96,487
Universal gas constant, R (J/mol-K)	8.314
Relative humidity for anode/cathode	1

2.3. Proton exchange membrane electrolyzer (PEME) modeling

The energy requirement for the PEME can be defined by [18]:

$$\Delta H = \Delta G + T \Delta S \quad (23)$$

Here, signifies the required electrical energy (Gibb's free energy), while $T\Delta S$ represents the thermal energy needed for the process in units of J/mol H_2 . Thermodynamic tables are used to compute enthalpy (H), entropy (S), and Gibbs free energy (G) values for water, hydrogen, and oxygen electrolysis. The required equations for modeling PEME are provided in Table 4.

Table 4. Required Equations Related to PEME Modeling (temperature in unit of K) [19, 20]

Parameter	Equation
Molar flow rate of H_2	$\dot{N}_{H_2,out} = \frac{J}{2F} = \dot{N}_{H_2o,reacted}$
Molar flow rates of O_2 and water	$\dot{N}_{o_2,out} = \frac{J}{4F}, \dot{N}_{H_2o,out} = \dot{N}_{H_2o,in} - \frac{J}{2F}$
Power of the PEME	$\dot{W}_{PEME} = J_{PEME} V_{PEME}, V_{PEME} = V_o + V_{act,c} + V_{act,a} + V_{ohm}$
Local ionic conductivity	$\sigma_{PEME} [\lambda(x)] = [0.5139.\lambda(x) - 0.326].\exp\left[1268.\left(\frac{1}{303} - \frac{1}{T}\right)\right]$
Water content	$\lambda(x) = \frac{\lambda_a - \lambda_c}{D}.x + \lambda_c$
Overall ohmic resistance	$R_{PEME} = \int_0^D \frac{dx}{\sigma_{PEME} [\lambda(x)]}$
Nernst voltage	$V_o = 1.229 - 8.5.10^{-4}.(T_{PEME} - 298)$
Anode activation overpotential	$V_{act,a} = \frac{RT}{F} \cdot \sinh^{-1}\left(\frac{J}{2.J_{o,a}}\right), J_{o,a} = J_a^{ref} \cdot \exp\left(\frac{-E_{act,a}}{RT}\right)$
Cathode activation overpotential	$V_{act,c} = \frac{RT}{F} \cdot \sinh^{-1}\left(\frac{J}{2.J_{o,c}}\right), J_{o,c} = J_c^{ref} \cdot \exp\left(\frac{-E_{act,c}}{RT}\right)$
Ohmic overpotential	$V_{ohmic} = R_{PEME} \cdot J$
Energy equation	$\dot{m}_9 h_9 + R_{PEME} = \dot{m}_{11} h_{11} + \dot{m}_{14} h_{14}$
Exergy equation	$\dot{E}x_9 + \dot{W}_{PEME} = \dot{E}x_{11} + \dot{E}x_{14} + \dot{E}x_d^{PEME}$

The input variables concerning the PEME modeling are presented in Table 5.

Table 5. Input Parameters for the PEM Electrolyzer

Parameter	Value	Parameter	Value
Active surface area of PEME (cm ²)	100	LHV_{H_2} (kJ/mol)	242.847
Inlet water temperature, T_{PEME} (K)	335	J_a^{ref} (A/m ²)	17×10^{-4}
Water content at anode, λ_a	14	J_c^{ref} (A/m ²)	4.5×10^3
Water content at cathode, λ_c	10	$E_{act,a}$ (J/mol)	76×10^3
Membrane thickness of PEME (cm)	0.005	$E_{act,c}$ (J/mol)	18×10^3
Limiting current density (A/cm ²)	2.0	Operating pressure, P_{PEME} (kPa)	101
Current density of PEME, (A/cm ²)	0.4	Electrons transfer coefficient	0.3

To assess the accuracy of the numerical model of the PEM electrolyzer, a comparison is made with experimental data from Ni et al. [21], as depicted in Fig. 7. This comparison aims to gauge the model’s precision to predict PEME behavior and performance.

The strong alignment between numerical and experimental data in Fig. 7 indicates the model’s substantial reliability in accurately predicting PEM electrolyzer performance.

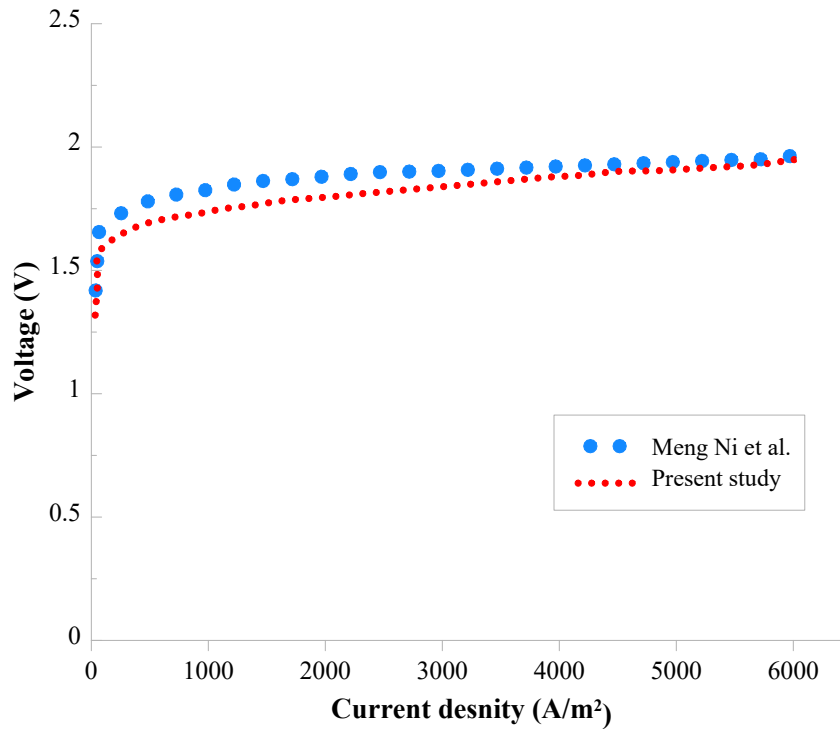


Fig. 7. Comparing the present study and reported literature results for PEM electrolyzer performance.

2.4. Organic Rankine cycle (ORC) modeling

To perform a thermodynamic analysis and model the

ORC, we treat the turbine, pump, evaporator, and condenser as separate control volumes. Each component utilizes specific correlations, which are detailed in Table 6.

Table 6. Thermodynamic Equations for the ORC Components [22]

Component	Energy equation	Exergy equation
Evaporator	$\dot{m}_7 h_7 + \dot{m}_2 h_2 = \dot{m}_5 h_5 + \dot{m}_3 h_3$	$\dot{E}x_7 + \dot{E}x_2 = \dot{E}x_5 + \dot{E}x_3 + \dot{E}x_D^{Evap}$
Turbine	$\dot{m}_3 h_3 = \dot{m}_4 h_4 + \dot{W}_T$	$\dot{E}x_3 = \dot{E}x_4 + \dot{W}_T + \dot{E}x_D^T$
Condenser	$\dot{m}_4 h_4 + \dot{m}_{16} h_{16} = \dot{m}_1 h_1 + \dot{m}_{17} h_{17}$	$\dot{E}x_4 + \dot{E}x_{16} = \dot{E}x_1 + \dot{E}x_{17} + \dot{E}x_D^{Cond}$
Pump	$\dot{m}_1 h_1 + \dot{W}_P = \dot{m}_2 h_2$	$\dot{E}x_1 + \dot{W}_P = \dot{E}x_2 + \dot{E}x_D^P$

The input variables for ORC are provided in Table 7.

Table 7. Input Parameters for ORC and Circulation Water [23]

Parameter	Value
Pressure of circulation water, P_{CW} (kPa)	101
$T_{PEMFC} - T_6$	2
Inlet pressure of turbine, P_3 (kPa)	512
Condensation temperature, T_{cond} (K)	313
Condensation pressure, T_{cond} (kPa)	249
Condenser cooling water inlet temperature, T_{16} (K)	T_{amb}
(K)	5
for evaporator and condenser (K)	5
Isentropic turbine efficiency (%)	80
Isentropic pump efficiency (%)	75

3. Results and discussion

Fig. 8 demonstrates the effects of different solar irradiances on the performance of the PV cell with a surface temperature of 45 °C. As it is depicted, elevated solar radiation is a pivotal factor that substantially enhances the power production of photovoltaic (PV) cells. This phenomenon can be clarified in a stepwise manner. Firstly, the increase in solar radiation corresponds to a heightened influx of photons onto the sur-

face of the PV cells. Each photon carries a quantifiable amount of energy contingent upon its specific wavelength. With the amplification of solar radiation, there is an augmented overall energy input into the PV cells. This heightened energy influx precipitates the excitation of electrons within the semiconductor material encompassed by the PV cells. These excited electrons gain greater kinetic energy, consequently generating a higher electric current. This electric current constitutes a fundamental component of the power output in the PV cells.

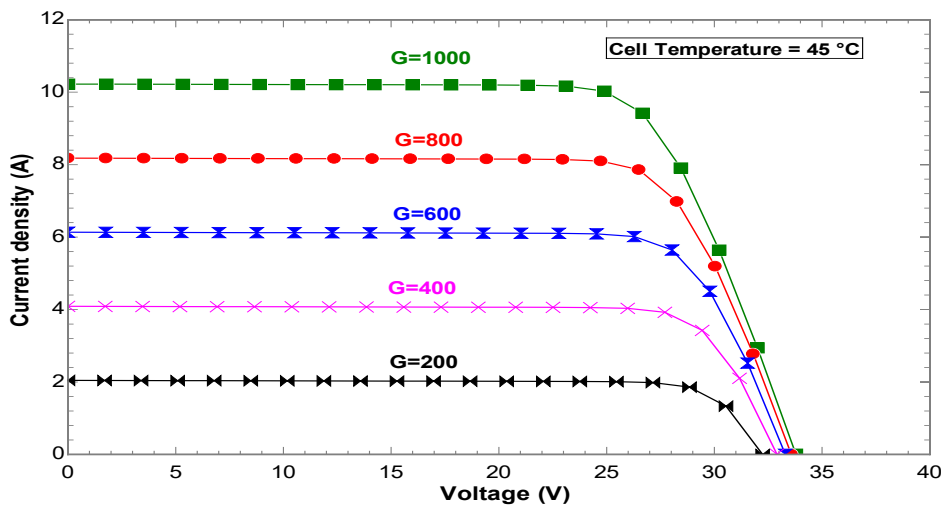


Fig. 8. The effects of different solar irradiances on the performance of the PV cell.

The influence of PEME's inlet water temperature on the performance of PEME is indicated in Fig. 9. Raising the inlet water temperature in a proton exchange membrane (PEM) electrolyzer has a notable impact on its energy efficiency and overall performance. The increase in water temperature reduces the electrical resistance of the water, lowering the voltage required for electrolysis. However, this also leads to excess en-

ergy dissipating as thermal energy (heat) into the water, diverting it from useful work. Consequently, the PEM electrolyzer becomes less energy-efficient as a larger portion of the input energy is lost as heat. This diminishes the overall performance of the electrolyzer in terms of its ability to efficiently produce hydrogen and oxygen from water.

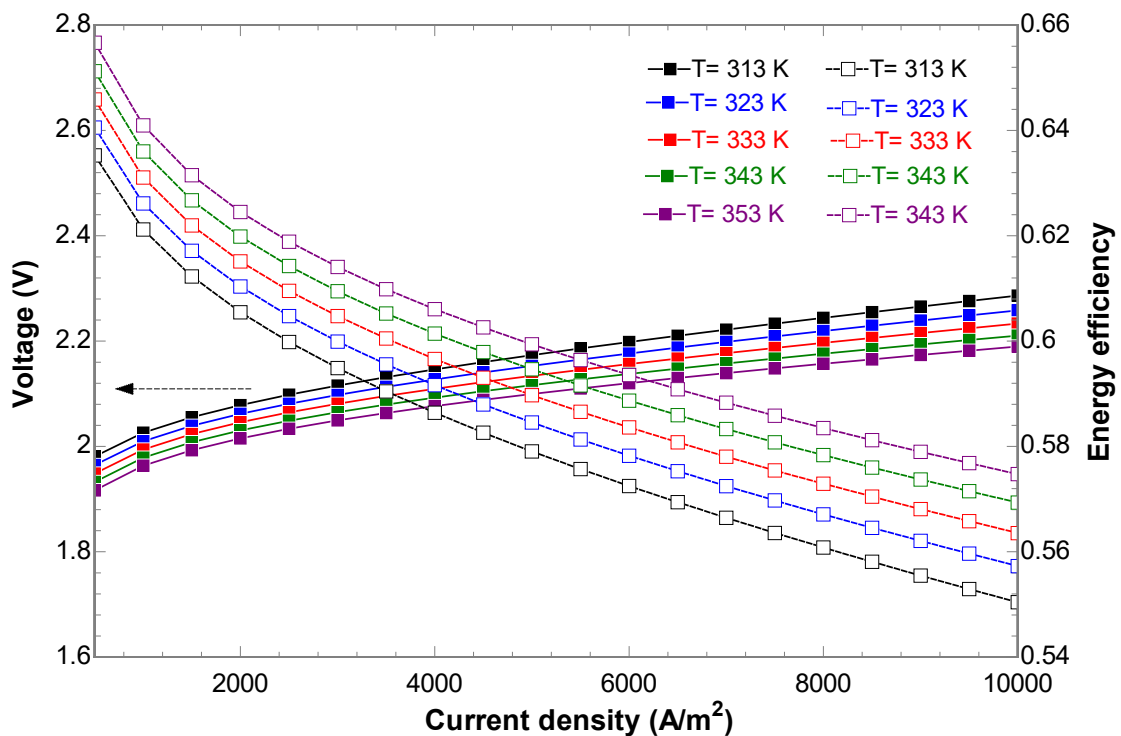


Fig. 9. The effects of PEME inlet water temperature on the performance of the PEME.

In Fig. 10 shows the effects of the different PEMFC operational temperatures. As can be seen, increasing the stack temperature in PEMFC has several advantages for energy efficiency and overall performance. It accelerates electrochemical reactions, reducing activation losses, and enhancing power output. Faster ion transport through the electrolyte improves conductivity, and improved water management prevents cell degradation. Moreover, higher temperatures widen the operating range, making the PEMFC more versatile for various applications and environments. However, it also

brings challenges like increased heat generation, water management issues, and durability concerns that can hamper performance. Therefore, striking the right balance between higher stack temperature and system reliability is paramount. The PEM fuel cell's peak productivity and overall energy efficiency and the entire system are achieved within the 620 to 820 mA/cm² range. Beyond this range, the overall energy efficiency of the system declines.

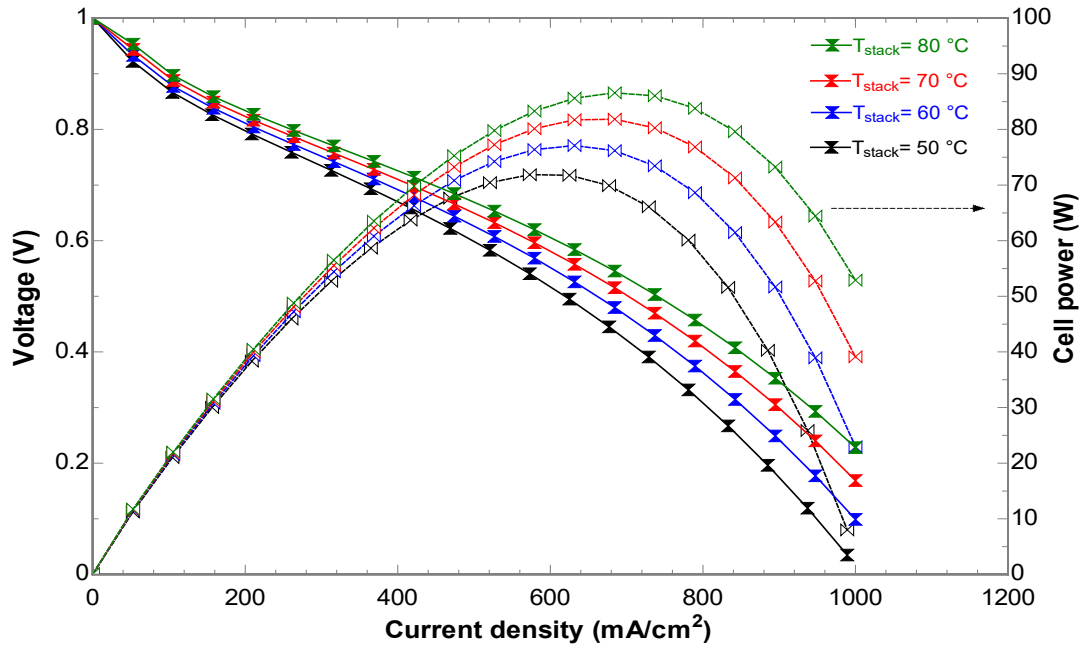


Fig. 10. The effects of PEMFC stack temperature on the performance of the PEMFC.

Fig. 11 illustrates the impacts of varying operational pressures on the PEMFC. Increasing the operational pressure in PEMFC offers several energy efficiency and overall performance benefits. It enhances gas diffusion, reduces mass transport limitations, and aids in more efficient water removal. These factors collectively improve reactant utilization and expand the

cell's operational range, enhancing PEMFC performance and energy efficiency. Similar to the impact of stack temperature, elevating the operational pressure presents challenges. Therefore, achieving the optimal balance between increased operational pressure and system reliability is of utmost importance.

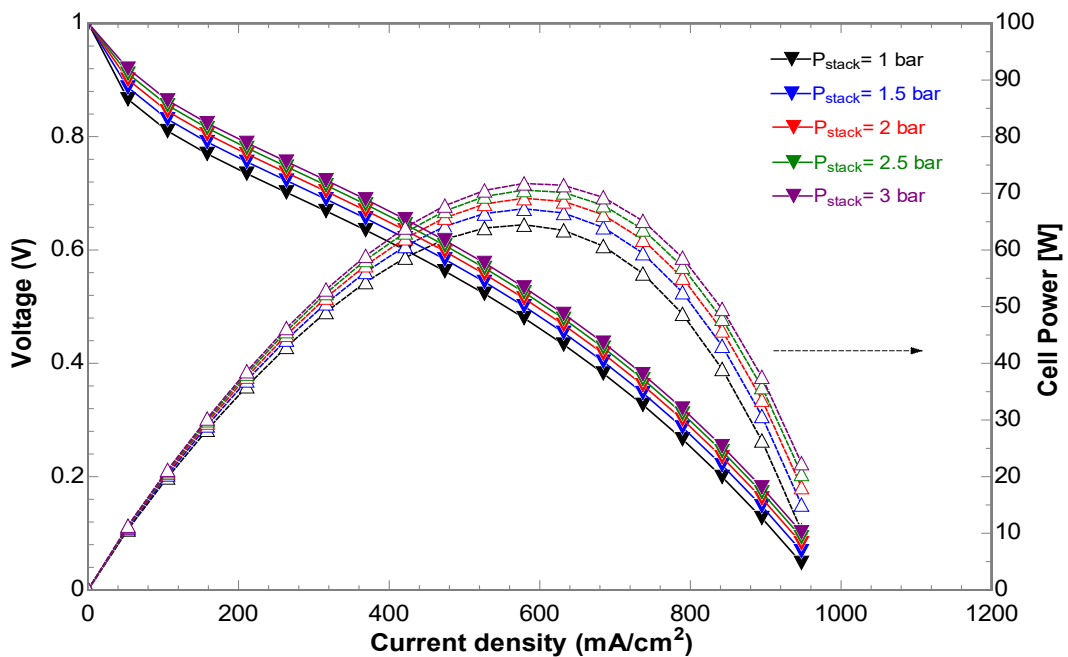


Fig. 11. The effects of PEMFC pressure on the performance of the PEMFC.

Increasing the inlet pressure of the Organic Rankine Cycle (ORC) turbine is a strategy that significantly bolsters the performance of the ORC subsystem. This boost in pressure brings about multiple advantages, primarily a marked improvement in energy efficiency and power generation. Consequently, the overall energy efficiency of the entire system experiences a noticeable upswing. However, an optimal inlet pres-

sure point for the ORC turbine exists, one at which the system's energy efficiency reaches its zenith. Remarkably, this optimum pressure is approximately 580 kPa. At this specific pressure level, the system operates at its most efficient state, extracting the highest possible performance from the ORC turbine and contributing to the overall energy efficiency of the entire system (see Fig. 12).

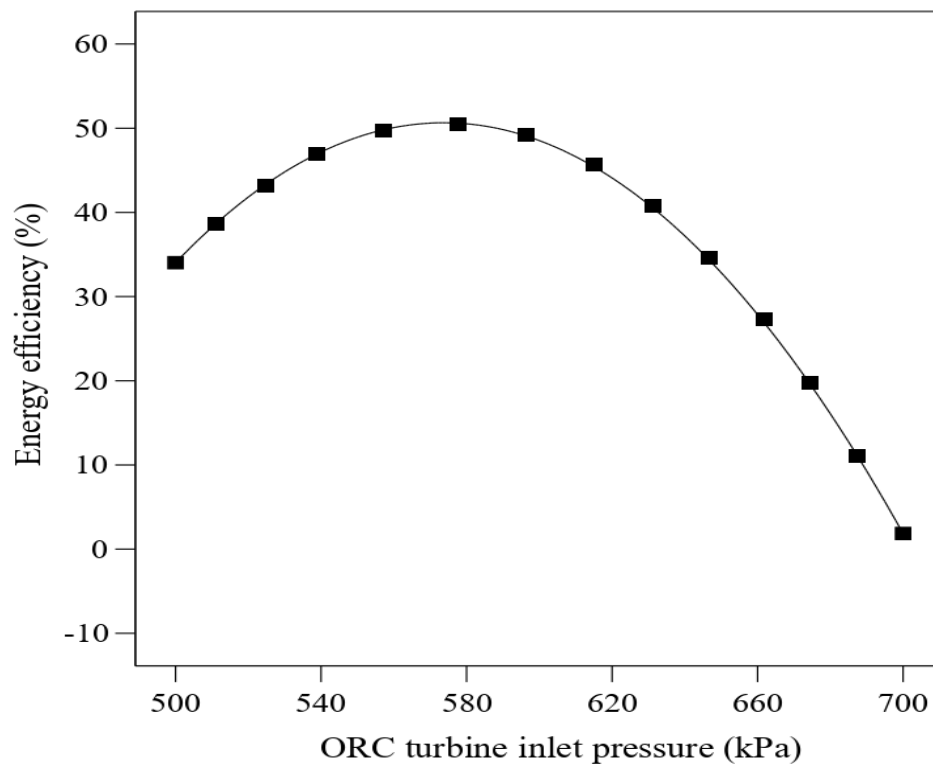


Fig. 12. The effects of ORC turbine inlet pressure on the overall system's energy efficiency.

The pressure ratio within the ORC subsystem plays a pivotal role in governing the expansion process, particularly during the phase change (vaporization) that propels the turbine. When the turbine's inlet pressure is elevated, it naturally corresponds to a more substantial pressure differential across the turbine, resulting in a markedly more efficient expansion process. This, in turn, mitigates exergy losses stemming from irreversibilities and amplifies power generation. Furthermore, the adjust-

ment of the ORC inlet turbine pressure holds sway over the energy efficiency of the cycle by influencing the alignment of heat source and sink temperatures. The specific characteristics of R245fa, the chosen working fluid, highlight the existence of an optimum inlet pressure for the ORC turbine. This particular pressure point leads to peak performance and the highest overall exergy efficiency, and it is situated at approximately 600 kPa, as shown in Figure 13.

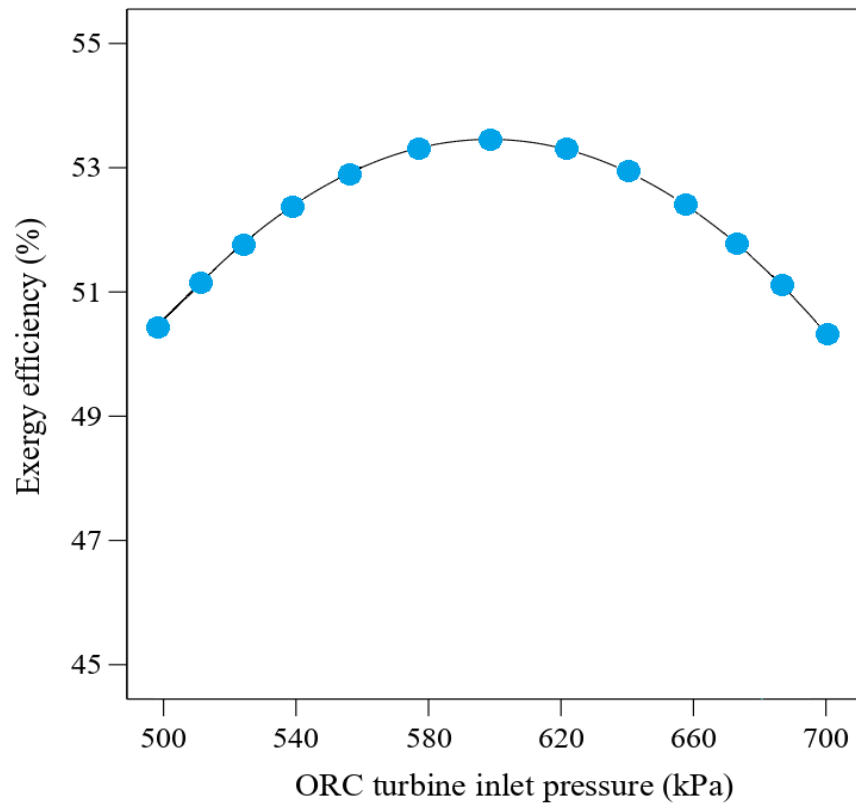


Fig. 12. The effects of ORC turbine inlet pressure on the overall system's exergy efficiency.

Table 8 presents a comparative assessment of the findings from this study and those available in the current literature. The outcomes of our energy and exergy analysis exhibit a satisfactory alignment with

the results reported in previous studies. Additionally, according to Table 8, it can be inferred that the ORC system has a significant effect on the performance of the proposed system.

Table 8. A Comparison of System Configuration and Performance for the Present Study and the Literature.

Ref.	System configuration	η	ψ
[7]	PV/battery/FC/electrolyzer/biogas	25%	N.A
[24]	PV/FC/electrolyzer	20.4%	21.8%
[25]	PV/battery/FC/electrolyzer	9%	N.A
[26]	PV/battery/FC/electrolyzer	1.5%	2.0%
[27]	PTC/FC/electrolyzer/Rankine cycle	N.A	17.6%
This study	PV/battery/FC/electrolyzer/ORC	50.9%	54.7%

Conclusions

In this current study, we have designed an off-grid hybrid energy system that comprises a photovoltaic (PV) unit, a proton exchange membrane (PEM) fuel cell, a proton exchange membrane electrolyzer (PEME), and an Organic Rankine Cycle (ORC). The primary aim was to ensure a continuous power supply to meet the uninterrupted load requirements of a telecommunications tower. The key outcomes of this research are outlined as follows:

- Increased solar radiation significantly enhances the power production of a PV cell, as it leads to greater photon influx, excitation of electrons, and subsequent higher electric current output.
- Raising the inlet water temperature in the PEME lowers the voltage required for electrolysis but results in excess energy dissipation as heat, reducing overall energy efficiency.
- Elevating the stack temperature in the PEMFC accelerates electrochemical reactions, improves ion transport, and widens the operational range, benefiting energy efficiency and performance.
- The operational pressure in the PEMFC affects gas diffusion, mass transport, and water removal, enhancing reactant utilization and overall performance. However, achieving the right balance between increased pressure and system reliability is crucial.
- Increasing the inlet pressure of the ORC turbine enhances the ORC subsystem's performance, improving energy efficiency and power generation. The optimum inlet pressure for peak system efficiency is around 580 kPa.
- The pressure ratio within the ORC subsystem influences the expansion process, with higher inlet pressure resulting in a more efficient expansion and reduced exergy losses. An optimal inlet pressure of approximately 600 kPa maximizes overall exergy efficiency.

References

- [1] Ma, X., et al., (2023). What changes can solar and wind power bring to the electrification of China compared with coal electricity: From a cost-oriented life cycle impact perspective. *Energy Conversion and Management*, . 289: p. 117162.
- [2] Xu, A., et al., (2023). Thermodynamic analyses of an innovative system combined dehumidification, cooling and heating driven by solar energy. *Energy Conversion and Management*, . 279: p. 116757.
- [3] Xue, X., et al., (2023). Proposal and evaluation of a hydrogen and electricity cogeneration system based on thermochemical complementary utilization of coal and solar energy. *Energy Conversion and Management*, . 291: p. 117266.
- [4] Song, H., et al., (2023). Analysis of cascade and hybrid processes for hydrogen production by full spectrum solar energy utilization. *Energy Conversion and Management*, . 291: p. 117289.
- [5] Bilen, K. and İ. (2023). Erdoğan, Effects of cooling on performance of photovoltaic/thermal (PV/T) solar panels: A comprehensive review. *Solar Energy*, . 262: p. 111829.
- [6] Basnet, S., et al., (2023). A review on recent stand-alone and grid integrated hybrid renewable energy systems: System optimization and energy management strategies. *Renewable Energy Focus*, 46: p. 103-125.
- [7] Tiam Kapen, P., et al., (2022). Techno-economic feasibility of a PV/battery/fuel cell/electrolyzer/bio-gas hybrid system for energy and hydrogen production in the far north region of cameroon by using HOMER pro. *Energy Strategy Reviews*, . 44: p. 100988.

- [8] Salari, A., et al., (2023). Optimization of a solar-based PEM methanol/water electrolyzer using machine learning and animal-inspired algorithms. *Energy Conversion and Management*, 283: p. 116876.
- [9] Xiao, C., et al., (2023) . Design of a novel fully-active PEMFC-Lithium battery hybrid power system based on two automatic ON/OFF switches for unmanned aerial vehicle applications. *Energy Conversion and Management*, 292: p. 117417.
- [10] Li, N., Z. Lukszo, and J. Schmitz, (2023). An approach for sizing a PV–battery–electrolyzer–fuel cell energy system: A case study at a field lab. *Renewable and Sustainable Energy Reviews*, . 181: p. 113308.
- [11] Šimunović, J., G. Radica, and F. Barbir,(2023). The effect of components capacity loss on the performance of a hybrid PV/wind/battery/hydrogen stand-alone energy system. *Energy Conversion and Management*,. 291: p. 117314.
- [12] Mohammed, A., et al.,(2023). A multi-objective optimization model based on mixed integer linear programming for sizing a hybrid PV-hydrogen storage system. *International Journal of Hydrogen Energy*, 48(26): p. 9748-9761.
- [13] Remund, J., et al., (2020). Meteororm version 8. *METEOTEST* (www.meteotest.com).
- [14] Duffie, J.A., W.A. Beckman, and N. Blair,(2020). Solar engineering of thermal processes, photovoltaics and wind. : *John Wiley & Sons*.
- [15] Rahimi-Esbo, M., A.R. Sangtabi, and E. Alizadeh, (2022)). Manifold Design in a PEM Fuel Cell Stack to Improve Flow Distribution Uniformity. *Sustainability*, . 14(23): p. 15702.
- [16]. Eslami, N., et al., (2023). Experimental Analysis of Large Active Area Polymer Electrolyte Membrane Fuel Cell Stack for Determining Optimal Operating Conditions. *Arabian Journal for Science and Engineering*.
- [17] Rahimi-Esbo, M., et al.,(2020). Novel design and numerical evaluating of a cooling flow field in PEM-FC with metallic bipolar plates. *International Journal of Hydrogen Energy*,
- [18] Oh, D., D.-S. Cho, and T.-W. Kim, (2023). Design and evaluation of hybrid propulsion ship powered by fuel cell and bottoming cycle. *International Journal of Hydrogen Energy*, 48(22): p. 8273-8285.
- [19] Liu, S., et al., (2023). Multi-objective optimization of proton exchange membrane fuel cell geometry and operating parameters based on three new performance evaluation indexes. *Energy Conversion and Management*, 277: p. 116642.
- [20] Etghani, M.M. and H. Boodaghi, (2023). Design and Performance Assessment of a Novel Poly-generation System with Stable Production of Electricity, Hydrogen, and Hot Water: Energy and Exergy Analyses. *Arabian Journal for Science and Engineering*, .
- [21] Ni, M., M.K.H. Leung, and D.Y.C. Leung, (2008). Energy and exergy analysis of hydrogen production by a proton exchange membrane (PEM) electrolyzer plant. *Energy Conversion and Management*, . 49(10): p. 2748-2756.
- [22] Boodaghi, H., M.M. Etghani, and K. Sedighi, (2022)). A novel investigation of waste heat recovery from a stationary diesel engine using a dual-loop organic Rankine cycle. *Journal of the Brazilian Society of Mechanical Sciences and Engineering*, . 44(8): p. 369.
- [23] Boodaghi, H., M.M. Etghani, and K. Sedighi,

(2022). Advanced Exergy Scrutiny of a Dual-loop Organic Rankine Cycle for Waste Heat Recovery of a Heavy-duty Stationary Diesel Engine. *International Journal of Engineering*, . 35(4): p. 644-656.

[24] Shaygan, M., et al., (2019). Energy, exergy, advanced exergy and economic analyses of hybrid polymer electrolyte membrane (PEM) fuel cell and photovoltaic cells to produce hydrogen and electricity. *Journal of Cleaner Production*, . 234: p. 1082-1093.

[25] Jafari, M., et al., (2019). Thermoeconomic analysis of a standalone solar hydrogen system with hybrid energy storage. *International Journal of Hydrogen Energy*, 44(36): p. 19614-19627.

[26] Ogbonnaya, C., A. Turan, and C.(2019). Abeykoon, Energy and exergy efficiencies enhancement analysis of integrated photovoltaic-based energy systems. *Journal of Energy Storage*, 26: p. 101029.

[27] Razmi, A.R., et al., (2022). A green hydrogen energy storage concept based on parabolic trough collector and proton exchange membrane electrolyzer/fuel cell: Thermodynamic and exergoeconomic analyses with multi-objective optimization. *International Journal of Hydrogen Energy*, . 47(62): p. 26468-26489.